

¹¹¹In-Cetuximab-F(ab')₂ SPECT and ¹⁸F-FDG PET for Prediction and Response Monitoring of Combined-Modality Treatment of Human Head and Neck Carcinomas in a Mouse Model

Laura K. van Dijk^{1,2}, Otto C. Boerman², Gerben M. Franssen², Johannes H.A.M. Kaanders¹, and Johan Bussink¹

¹Department of Radiation Oncology, Radboud University Medical Center, Nijmegen, The Netherlands; and ²Department of Radiology and Nuclear Medicine, Radboud University Medical Center, Nijmegen, The Netherlands

Treatment of head and neck squamous cell carcinomas with radiotherapy and the epidermal growth factor receptor (EGFR) inhibitor cetuximab shows an improved response in a subgroup of patients. The aim of this study was to noninvasively monitor treatment response by visualizing systemically accessible EGFR with ¹¹¹In-cetuximab-F(ab')₂ while simultaneously evaluating tumor metabolism with ¹⁸F-FDG PET during combined-modality treatment. **Methods:** Eighty mice with patient-derived head and neck squamous cell carcinomas xenografts, SCCNij202 or SCCNij185, were imaged with SPECT/CT using ¹¹¹In-cetuximab-F(ab')₂ (5 µg, 28 ± 6.1 MBq, 24 h after injection), followed by PET imaging with ¹⁸F-FDG (9.4 ± 2.9 MBq, 1 h after injection). Scans were acquired on mice 10 d before treatment with either single-dose irradiation (10 Gy), cetuximab alone, or cetuximab-plus-irradiation combined or on untreated control mice. Scans were repeated 18 d after treatment. Tumor growth was monitored up to 120 d after treatment. EGFR expression was evaluated immunohistochemically. **Results:** SCCNij202 responded to combined treatment ($P < 0.01$) and cetuximab treatment alone ($P < 0.05$) but not to irradiation alone ($P = 0.13$). SCCNij185 responded to combined treatment ($P < 0.05$) and irradiation ($P < 0.05$) but not to cetuximab treatment alone ($P = 0.34$). ¹¹¹In-cetuximab-F(ab')₂ uptake (tumor-to-liver ratio, scan 2 – scan 1) predicted response to therapy. A positive response to treatment significantly correlated with a reduced tracer uptake in the tumor in the second SPECT scan, compared with the first scan ($P < 0.005$ and < 0.05 for SCCNij202 and SCCNij185, respectively). Resistance to therapy was characterized by a significantly increased ¹¹¹In-cetuximab-F(ab')₂ tumor uptake; tumor-to-liver ratio was 2.2 ± 0.6 to 3.5 ± 1.2 , $P < 0.01$, for (irradiated) SCCNij202 and 1.4 ± 0.4 to 2.0 ± 0.3 , $P < 0.05$, for (cetuximab-treated) SCCNij185, respectively. ¹⁸F-FDG PET tumor uptake (maximum standardized uptake value, scan 2 – scan 1) correlated with tumor response for SCCNij202 ($P < 0.01$) but not for SCCNij185 ($P = 0.66$). EGFR fractions were significantly different: 0.9 ± 0.1 (SCCNij202) and 0.5 ± 0.1 (SCCNij185) ($P < 0.001$). The EGFR fraction was significantly lower for irradiated SCCNij202 tumors than for controls ($P < 0.005$). **Conclusion:** ¹¹¹In-cetuximab-F(ab')₂ predicted and monitored the effects of EGFR inhibition or irradiation during treatment in both head and neck carcinoma models investigated, whereas ¹⁸F-FDG PET only correlated with tumor response in the SCCNij202 model. Thus, the additional value of the ¹¹¹In-cetuximab-F(ab')₂ tracer is emphasized

and the tracer can aid in evaluating future treatments with EGFR-targeted therapies.

Key Words: SPECT; PET; radiotherapy; cetuximab; HNSCC

J Nucl Med 2015; 56:287–292

DOI: 10.2967/jnumed.114.148296

Squamous cell carcinoma of the head and neck is the sixth leading cause of cancer death worldwide (1). Risk factors include alcohol and tobacco use and oral infection by HPV (2). Treatment of advanced disease primarily consists of concurrent chemotherapy and radiotherapy. This combined treatment has improved outcome, albeit only modestly, but also increases treatment-related morbidity (3,4). Cetuximab, an epidermal growth factor receptor (EGFR) inhibitor, has been shown to significantly improve overall survival and locoregional control through radiosensitization with limited long-term morbidity (5,6). However, only a fraction of the patients will benefit from the addition of cetuximab treatment, and before treatment it is unclear which patients are most likely to benefit. Patient stratification is pivotal to improve clinical response rates, and biomarker development for prediction or response to treatment is widely investigated.

A proposed biomarker in HNSCC is tumor EGFR expression because the EGFR is significantly overexpressed, compared with normal epithelial tissues (7). However, in a phase II study by Wierzbiicki et al., it was shown that even without detectable EGFR, cetuximab as a monotherapy for colorectal carcinomas could be clinically effective and recently, an inverse relationship between EGFR expression and response was noted by Hartmann et al. (8,9). Nuclear medicine imaging advances on biopsy/single cell-dependent techniques because it allows the noninvasive assessment of the EGFR in the intact tumor, accounting for intratumoral variables such as vasculature, blood supply, and interstitial fluid pressure. Additionally, imaging can be repeated during treatment and serve as a monitoring tool. Several PET markers such as ¹⁸F-FDG, 3'-deoxy-3'-¹⁸F-fluorothymidine, and ¹⁸F-fluoromisonidazole have been investigated in HNSCC patients and have shown prognostic value (10–12) but do not aid in treatment selection. In previous studies, an anti-EGFR tracer, ¹¹¹In-cetuximab-F(ab')₂, was developed and evaluated in several preclinical setups. It has been shown to visualize systemically accessible EGFR in multiple HNSCC models and the change in accessible EGFR in response to single-dose irradiation (13,14). Here, we assess its potential relevance in 2 HNSCC xenograft models and include 3 treatment arms—irradiation,

Received Sep. 9, 2014; revision accepted Dec. 8, 2014.

For correspondence or reprints contact: Laura K. van Dijk, Department of Radiation Oncology, Radboud University Medical Center, P.O. Box 9101, 6500 HB Nijmegen, The Netherlands.

E-mail: laura.vandijk@radboudumc.nl

Published online Dec. 31, 2014.

COPYRIGHT © 2015 by the Society of Nuclear Medicine and Molecular Imaging, Inc.

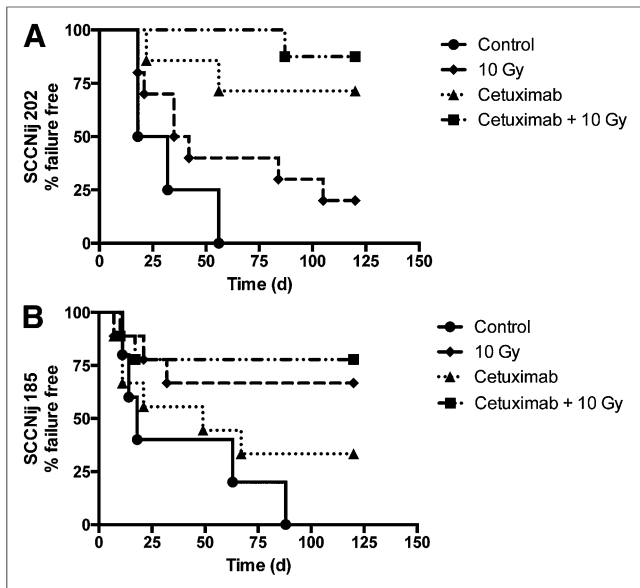


FIGURE 1. Kaplan–Meier survival curves showing response to cetuximab or irradiation in SCCNij202 (A) and SCCNij185 (B). Animals were treated with single irradiation dose of 10 Gy, single intraperitoneal injection of 1 mg of cetuximab, or combination of both or served as controls. $n = 10$ per treatment group per HNSCC tumor type.

cetuximab, and combination therapy—to evaluate its predictive value and its role in response monitoring.

MATERIALS AND METHODS

Tumor Models

Six- to 10-wk-old athymic BALB/c nu/nu mice were xenografted subcutaneously in the right hind leg with viable tumor tissue ($\sim 1 \text{ cm}^3$, $\sim 1 \times 10^6$ tumor cells) of the serial-passaged human HNSCC lines

SCCNij202 or SCCNij185. Animals were housed in filter-topped cages in accordance with institutional guidelines. Experiments started 3 wk (SCCNij202) or 8 wk (SCCNij185) after transplantation. The Animal Welfare Committee of the Radboud University Medical Center approved the animal experiments.

Experimental Setup

For each tumor model, 60 animals (total $n = 120$) were assigned into 4 treatment groups: radiotherapy, cetuximab, cetuximab combined with radiotherapy, and control ($n = 15$ per group). Tumor volume was estimated using the formula $4/3 \pi \times r_1 \times r_2 \times r_3$. For growth delay, tumors were measured twice a week, and the endpoint was reached when tumor volume doubled (SCCNij185) or tripled (SCCNij202) in size, compared with start volume. Different endpoints were chosen for both tumor models because SCCNij202 had a shorter doubling time than SCCNij185. Maximum follow-up time was 120 d. Nonresponders were defined as those reaching tumor doubling or tripling of start volume. A reduction in tumor size or growth delay (below doubling or tripling volume) was considered a response of the tumor to therapy.

Baseline ^{111}In -cetuximab- F(ab')_2 SPECT/CT and ^{18}F -FDG PET scans of 80 mice were acquired 10 d before treatment. Radiotherapy consisted of a single dose of 10-Gy x-rays on the tumor-bearing right hind leg (320 kV; dose rate, 3.8 Gy/min; X-RAD [RPS Services Limited]). Mice received a therapeutic dose of 1.0 mg of cetuximab by intraperitoneal injection, 3 d before radiotherapy. Eighteen days after treatment, all mice were subjected to a second SPECT and PET scan and followed in a growth delay setup. From the remaining 40 mice, 5 (SCCNij202) or 4 (SCCNij185) of each group were euthanized for immunohistologic evaluation 18 d after treatment.

SPECT and PET Imaging

^{111}In -cetuximab- F(ab')_2 (specific activity, 400 GBq/ μmol ; radiochemical purity, $>95\%$) was produced as described previously (14). SPECT images were acquired 24 h after intravenous injection with ^{111}In -cetuximab- F(ab')_2 ($5 \mu\text{g}$, $28 \pm 6.1 \text{ MBq}$, 200 μL per mouse) using an ultra-high-resolution animal SPECT/CT scanner (USPECT-II; MILabs). Mice were scanned in a prone position under general anesthesia (isoflurane/compressed air) using the 1.0-mm-diameter multipinhole collimator tube. SPECT scans were acquired for 60 min, followed by a 180-s CT scan. Subsequently, mice were injected with ^{18}F -FDG ($9.4 \pm 2.9 \text{ MBq}$) (GE Healthcare) and kept under general anesthesia for 1 h before 20-min PET imaging with an Inveon small-animal PET scanner (Siemens Preclinical Solutions) was started, followed by a 400-s transmission scan using the built-in ^{57}Co source (energy window, 120–125 keV) for attenuation correction.

Excised tumors were snap-frozen in liquid nitrogen for immunohistochemical staining purposes. Because of technical issues with the scanners, not all mice could be scanned at the second time point.

Immunohistochemistry

Frozen tumor sections (5 μm) were cut and mounted on poly-L-lysine-coated slides for immunohistochemistry. First, tumor sections were fixed in acetone in 4°C for 10 min. Subsequently, slides were washed and stained for EGFR, vessels, and nuclei. Primary and secondary antibodies were diluted in primary antibody diluent (Abcam). Between all consecutive steps of the staining process, sections were rinsed

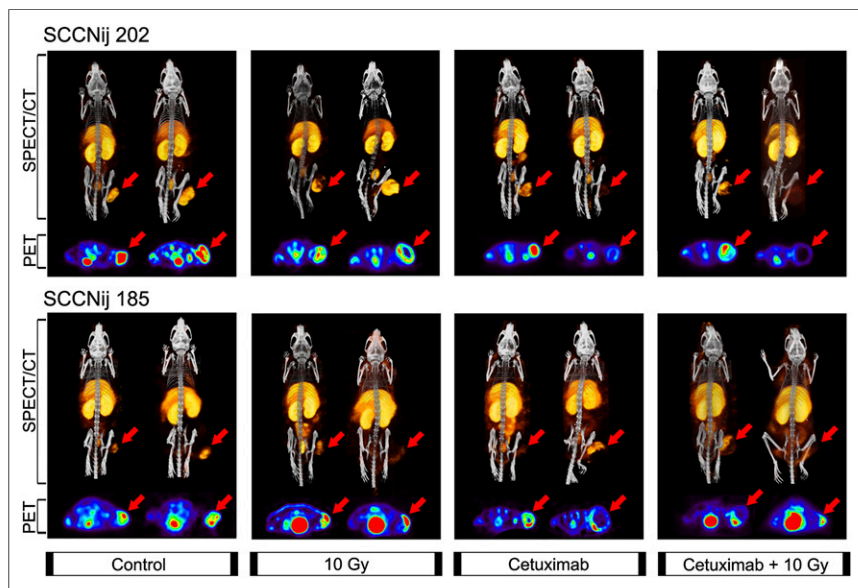


FIGURE 2. ^{111}In -cetuximab- F(ab')_2 (dorsal view, 24 h after injection) and ^{18}F -FDG (transversal view, 1 h after injection) uptake. (Upper) SCCNij202. (Lower) SCCNij185. Per treatment group, baseline example (left, 10 d before treatment) and treated sample (right, 18 d after treatment) are shown. Tumors are located on right hind leg (red arrow). Background uptake was present in SPECT images (liver, kidneys, bladder) and PET (bladder).

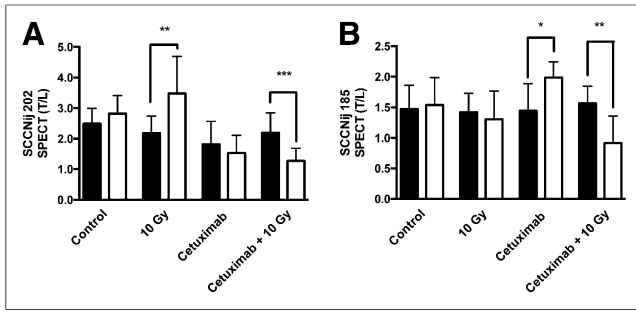


FIGURE 3. ^{111}In -cetuximab- $\text{F}(\text{ab}')_2$ tumor uptake shown as SPECT T/L ratio for SCCNij202 (A) and SCCNij185 (B). Mice were imaged 10 d before (black bars) and 18 d after (white bars) treatment with cetuximab or irradiation. $n = 10$ per treatment group per HNSCC tumor type. * $P < 0.05$. ** $P < 0.01$. *** $P < 0.001$.

3 times for 5 min in 0.1 M phosphate-buffered saline, pH 7.4 (Klinipath).

After rehydration in phosphate-buffered saline, sections were incubated with goat anti-EGFR antibody, 1:50 (Santa Cruz Biotechnology Inc.) and subsequently with donkey antigoat Cy3, 1:600 (Jackson ImmunoResearch). To stain the blood vessels, all sections were incubated with undiluted 9F1 supernatant (antimouse endothelium) (15) for 45 min at 37°C, followed by incubation with chicken antirat-Alexa647, 1:100 (Invitrogen Molecular Probes). All nuclei were stained with Hoechst 33342 (0.5 $\mu\text{g}/\text{mL}$; Sigma), after which slides were mounted in Fluorostab (ICN Biomedicals). One adjacent section per tumor was hematoxylin and eosin-stained to help distinguish necrotic areas and nontumor tissue from viable tumor areas.

Image Analysis

SPECT scans were reconstructed with MILabs reconstruction software, using an ordered-expectation maximization algorithm with a voxel size of 0.375 mm. Tumor-to-liver pixel value (T/L) ratios were determined by drawing regions of interest (ROIs) around the tumor (thresholded at 40% of the maximum signal) and within the liver (Inveon Research Workplace software, version 4.0; Siemens Preclinical Solutions). The relative difference between T/L ratios from the first and second scan is represented as $(\text{scan } 2 - \text{scan } 1)/\text{scan } 1$.

PET images were reconstructed using an ordered-subset expectation maximization 3-dimensional algorithm of 2 iterations, followed by maximum a posteriori (18 iterations, uniform variance smoothing factor $[\beta] = 0.05$) reconstruction optimized for uniform resolution (Inveon Acquisition Workplace, version 1.5; Siemens Preclinical Solutions). PET images were analyzed using Siemens Inveon Research Workplace software (version 4.0; Siemens Preclinical Solutions). ROIs were manually drawn around the tumor. Tumors were thresholded at 50% of the maximum signal. Quantification of tracer uptake in tumor ROIs of the attenuation-corrected slices was obtained by calculating the maximum standardized uptake values (SUV_{max}) by correcting for the injected activity, injection time, and body weight. The relative difference between the SUV_{max} from the first and second scan is represented as $(\text{scan } 2 - \text{scan } 1)/\text{scan } 1$.

After immunohistochemical staining, tumor sections were analyzed using a digital image analysis system, as described previously (16). In short, whole-tissue sections were scanned (magnification, $\times 10$; Axioskop [Zeiss]), and gray-scale images (pixel size, $2.59 \times 2.59 \mu\text{m}$) were obtained for EGFR, vessels, and nuclei and subsequently converted into binary images. The amount of positive pixels for EGFR staining was divided by total tumor area, providing the fraction of EGFR (fEGFR) using ImageJ software (version 1.43m, JAVA-based image-processing package).

Mean intensity of the EGFR staining (fEGFR) was determined by dividing EGFR pixel gray values (range, 0–4,095; 12 bits) by positive EGFR staining area. Thresholds for segmentation of the fluorescent signals were set above the background staining for each marker. Areas of necrosis were excluded from analysis by drawing ROIs.

Statistics

Statistical analyses were performed using Prism software (version 6.0e; GraphPad). The significance of tumor response was tested using Kaplan–Meier survival curves and Cox proportional hazards regression. The nonparametric Spearman or parametric Pearson test was used accordingly, and a P value of 0.05 or less was considered significant. Data are represented as mean \pm SD.

RESULTS

Growth Delay

Average tumor volume at onset of treatment was $228 \pm 101 \text{ mm}^3$ and $132 \pm 78 \text{ mm}^3$ for SCCNij202 and SCCNij185, respectively, and did not differ between treatment groups. SCCNij202 responded to combined ($P < 0.01$) and cetuximab treatment alone ($P < 0.05$) but not to irradiation ($P = 0.13$) (Fig. 1A). SCCNij185 responded to combined treatment ($P < 0.05$) and irradiation ($P < 0.05$) but not to cetuximab treatment alone ($P = 0.34$) (Fig. 1B).

^{111}In -Cetuximab- $\text{F}(\text{ab}')_2$ SPECT

^{111}In -cetuximab- $\text{F}(\text{ab}')_2$ tumor uptake decreased significantly in SCCNij202 and SCCNij185 tumors when a combined-modality treatment of cetuximab and single-dose 10-Gy irradiation within 2.5 wk after treatment was used ($P < 0.001$ and < 0.01 , respectively) (Figs. 2 and 3). Resistance to therapy—that is, lack of growth delay or increase in tumor volume up to 120 d—was characterized by a significantly increased ^{111}In -cetuximab- $\text{F}(\text{ab}')_2$ tumor uptake,

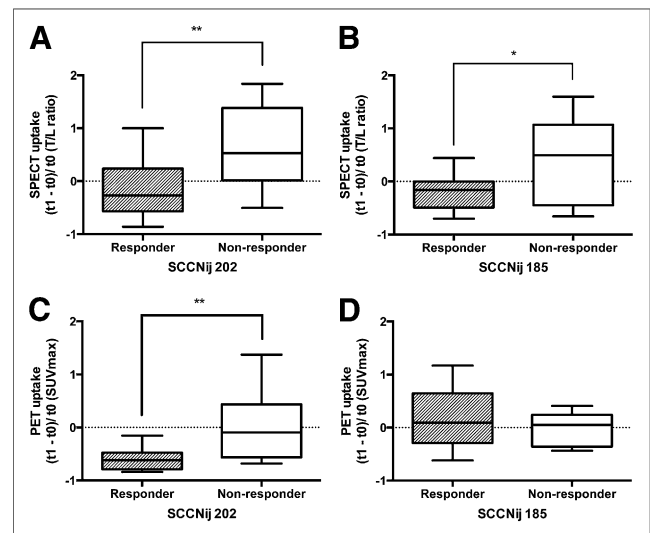


FIGURE 4. Relative T/L ratio of two ^{111}In -cetuximab- $\text{F}(\text{ab}')_2$ scans (A and B) and relative SUV_{max} ratio of two ^{18}F -FDG scans (C and D) dichotomized in responders and nonresponders. Positive response to treatment (left) significantly correlated with reduced ^{111}In -cetuximab- $\text{F}(\text{ab}')_2$ tracer uptake for SCCNij202 (A) and SCCNij185 (B). Positive response to treatment significantly correlated with reduced ^{18}F -FDG tracer uptake for SCCNij202 (C) but not for SCCNij185 (D). Horizontal lines represent grand mean. $t_0 = 10$ d before treatment; $t_1 = 18$ d after treatment. ** $P < 0.005$. * $P < 0.05$.

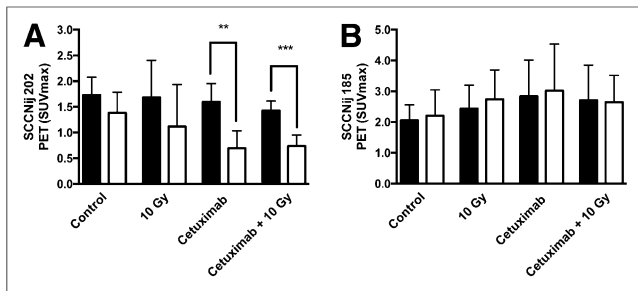


FIGURE 5. ^{18}F -FDG tumor uptake (SUV_{max}) for SCCNij202 (A) and SCCNij185 (B). Mice were imaged 10 d before (black bars) and 18 d after (white bars) treatment with cetuximab or irradiation. $n = 10$ per treatment group per HNSCC tumor type. ** $P < 0.01$. *** $P < 0.001$.

compared with the pretherapy scan, 18 d after treatment. The T/L ratio increased from 2.2 ± 0.6 to 3.5 ± 1.2 ($P < 0.01$) for (irradiated) SCCNij202 and from 1.4 ± 0.4 to 2.0 ± 0.3 ($P < 0.05$) for (cetuximab-treated) SCCNij185. Tumors that responded to therapy (those not reaching volume doubling or tripling, respectively) had a significantly reduced tracer uptake in the tumor in the second SPECT scan, compared with the first scan ($P < 0.005$ and < 0.05 for SCCNij202 and SCCNij185, respectively) (Figs. 4A and 4B).

^{18}F -FDG PET

^{18}F -FDG PET tumor uptake correlated with tumor response for SCCNij202 ($P < 0.005$) but not for SCCNij185 ($P = 0.66$) (Figs. 4C and 4D). The decrease of ^{18}F -FDG uptake in the tumor was significant for SCCNij202 tumors treated with cetuximab and with the combination therapy: 1.59 ± 0.36 to 0.70 ± 0.34 , $P < 0.005$, and 1.43 ± 0.18 to 0.74 ± 0.21 , $P < 0.0001$, respectively (Figs. 2 and 5).

Immunohistochemistry

The fEGFRs of SCCNij202 and SCCNij185 control tumors obtained by quantification of EGFR by immunohistochemistry were significantly different: 0.9 ± 0.1 (SCCNij202) and 0.5 ± 0.1 (SCCNij185) ($P < 0.05$). fEGFR was significantly lower for irradiated SCCNij202 tumors than controls ($P < 0.005$) (Fig. 6A). The intensity of the EGFR staining was significantly elevated for irradiated SCCNij202 tumors ($P < 0.05$) (Fig. 6B). SCCNij185 did not show any significant differences between treated and control groups for fEGFR or iEGFR.

DISCUSSION

Stratification of patients could lead to an improved approach to treating heterogeneous diseases such as head and neck cancer. Here, we show that ^{111}In -cetuximab- $\text{F}(\text{ab}')_2$ can be an imaging biomarker for monitoring combined-modality treatment and predicts outcome to therapy in 2 head and neck tumor models.

The effectiveness of combining the EGFR inhibitor cetuximab with radiotherapy was established in the Bonner trial (5). The mechanism underlying this effect of cetuximab has been extensively studied and is in part mediated by inhibition of DNA damage repair after radiation-induced damage and by promoting apoptosis of the tumor cells (17–20). In our study, SCCNij202 and SCCNij185 tumors both responded to the combination therapy of cetuximab and irradiation. Treatment efficacy seemed to be facilitated by a greater

degree through EGFR inhibition for SCCNij202 as seen by the percentage of tumor response when given cetuximab alone. For SCCNij202, which has an increased EGFR gene copy number, it emphasizes the addiction to, and dependency on, EGFR ligands for continued proliferation and survival (21,22). A significant increase in ^{111}In -cetuximab- $\text{F}(\text{ab}')_2$ uptake in the tumor 2.5 wk after treatment was seen in tumors resistant to therapy. For radiation-resistant SCCNij202, we found an increase of tracer uptake in irradiated tumors along with an increase in iEGFR, which points to an increase in membrane receptor availability, as described previously (23). This increase of tumor uptake may represent a compensation mechanism for which the increase in systemically available EGFR enhances EGFR signaling promoting cell survival, especially in a heavily EGFR-reliant tumor model such as SCCNij202. For the SCCNij202 cetuximab-treated group, showing a good response to treatment, we observed no significant change in tumor fEGFR, iEGFR, or ^{111}In -cetuximab- $\text{F}(\text{ab}')_2$ tracer uptake after treatment. Cetuximab therapy is known to induce internalization and degradation of the EGFR (24), but it has been suggested that the effectiveness of EGFR inhibitors depends more on inhibition of the protein kinase B (AKT) and extracellular signal-regulated kinase (ERK) downstream signaling rather than membranous downregulation of the EGFR (25). This mechanism would be in line with our findings in the cetuximab/combined therapy-treated SCCNij202 tumors, for which the expression of EGFR and tumor tracer uptake did not change.

SCCNij185 tumors showed a more classic response to therapy: cetuximab enhancing irradiation-induced damage to tumor cells, as SCCNij185 tumors were responsive to irradiation but not to cetuximab treatment alone. Resistance to cetuximab was characterized by a significant increase in ^{111}In -cetuximab- $\text{F}(\text{ab}')_2$ tumor uptake 18 d after treatment, though no differences in iEGFR or fEGFR were found, thereby differentiating from the mechanism proposed for SCCNij202. Our findings support the current understanding that EGFR expression levels, as determined immunohistochemically, cannot predict therapy response (26–28). Intracellular signaling routes can have a pivotal role independent of high EGFR expression on tumors. In several studies, the persistent activation of the mitogen-activated protein kinase (MAPK) or P13-K/AKT pathway has been shown to play an important role in EGFR inhibitor resistance (25,29,30). SCCNij185 is known to express high endogenous levels of phosphorylated AKT, which might explain the insensitivity toward cetuximab treatment in this model (21).

Because both SCCNij202 and SCCNij185 tumors respond to combination therapy but respond differently to single treatment,

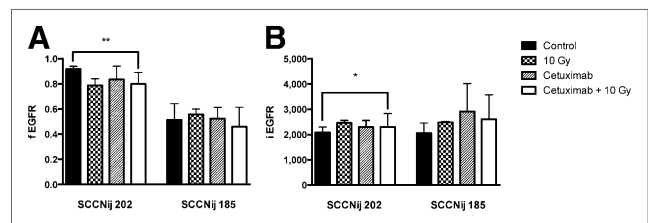


FIGURE 6. Immunohistochemical fEGFR (A) and iEGFR (B) for SCCNij202 and SCCNij185 tumors treated with cetuximab or irradiation. Significant decrease for fEGFR ($P < 0.001$) and increase for iEGFR ($P < 0.05$) were seen in irradiated SCCNij202 tumors. $n = 3$ –10 per treatment group per HNSCC tumor type.

initial ^{111}In -cetuximab-F(ab')₂ scans before treatment cannot be used as a marker for selection of EGFR inhibitor treatment. However, within 18 d after treatment, the difference in ^{111}In -cetuximab-F(ab')₂ uptake could predict tumor response, enabling the ability to monitor therapy response and thus modify the therapeutic regimen. Especially relevant is the increase of tracer uptake in the tumor as it correlates with nonresponders—that is, lack of growth delay or increase in tumor volume. More factors are necessary to predict individual response, as evidenced by the fact that some tumors show a decrease in tumor tracer uptake in the second scan but do not show a decrease in tumor size after therapy and vice versa. Interfering factors could include the amount of tumor necrosis, presence of edema, or variation in tumor size before start of treatment.

In a previous study, we assessed the response to irradiation with ^{111}In -cetuximab-F(ab')₂ imaging in SCCNij202 and SCCNij167 (23). As these 2 models portray clinical extremes in cetuximab response and high EGFR (SCCNij202) versus low EGFR (SCCNij167), it was deemed of added value to investigate a model with moderate EGFR expression and cetuximab nonresponse. In combination with the additional treatment regimens, which provide a more in-depth evaluation, this study elucidated the value of ^{111}In -cetuximab-F(ab')₂ imaging as it showed an increased tracer uptake in nonresponding tumors to different treatments in both SCCNij tumors.

In patients, response of HNSCC to chemoradiotherapy with imaging markers has been evaluated in several clinical studies (31). ^{18}F -FDG has been shown to have prognostic value, though the search for a predictive or early assessment potential has revealed conflicting results (32,33). In this study, a reduction in ^{18}F -FDG SUV_{max} correlated with tumor response and served as a predictive marker in SCCNij202 tumors, consistent with our previous findings (23). However, no difference in uptake was seen in SCCNij185 tumors, regardless of the applied treatment, emphasizing the need to apply tumor-specific tracers. Further investigation of additional early response and predictive markers for combined-modality treatment of radiotherapy with EGFR-inhibitors is warranted.

CONCLUSION

In this study, we have shown that ^{111}In -cetuximab-F(ab')₂ can be used to predict and monitor the effects of combined-modality treatment of EGFR inhibition and/or irradiation in 2 head and neck carcinoma models. Whereas ^{18}F -FDG PET correlated to tumor response in SCCNij202 only, the change in ^{111}In -cetuximab-F(ab')₂ uptake early after treatment correlated to treatment outcome in both SCCNij202 and SCCNij185. Most evident is the increased uptake in nonresponding tumors in the 2 tumor models, allowing visualization of tumor-specific ineffective therapies, hence facilitating early alterations in treatment regimen.

DISCLOSURE

The costs of publication of this article were defrayed in part by the payment of page charges. Therefore, and solely to indicate this fact, this article is hereby marked “advertisement” in accordance with 18 USC section 1734. This study was financially supported by a research grant of the Dutch Cancer Society (NKB-KUN 2010-4688). No other potential conflict of interest relevant to this article was reported.

ACKNOWLEDGMENTS

We thank Bianca Henk Arnts, Iris Lamers-Eleman, Kitty Lemmens-Hermans, Bianca Lemmers-de Weem, and Jasper Lok (Radboud University Medical Center) for their technical assistance.

REFERENCES

1. Ferlay J, Shin HR, Bray F, Forman D, Mathers C, Parkin DM. Estimates of worldwide burden of cancer in 2008: GLOBOCAN 2008. *Int J Cancer*. 2010;127:2893–2917.
2. Ragin CC, Modugno F, Gollin SM. The epidemiology and risk factors of head and neck cancer: a focus on human papillomavirus. *J Dent Res*. 2007;86:104–114.
3. Gao W, Li JZ, Ho WK, Chan JY, Wong TS. Biomarkers for use in monitoring responses of nasopharyngeal carcinoma cells to ionizing radiation. *Sensors (Basel)*. 2012;12:8832–8846.
4. Patel AN, Mehnert JM, Kim S. Treatment of recurrent metastatic head and neck cancer: focus on cetuximab. *Clin Med Insights Ear Nose Throat*. 2012;5:1–16.
5. Bonner JA, Harari PM, Giralt J, et al. Radiotherapy plus cetuximab for squamous-cell carcinoma of the head and neck. *N Engl J Med*. 2006;354:567–578.
6. Dittmann K, Mayer C, Rodemann HP. Inhibition of radiation-induced EGFR nuclear import by C225 (cetuximab) suppresses DNA-PK activity. *Radiother Oncol*. 2005;76:157–161.
7. Grandis JR, Tweardy DJ. Elevated levels of transforming growth factor alpha and epidermal growth factor receptor messenger RNA are early markers of carcinogenesis in head and neck cancer. *Cancer Res*. 1993;53:3579–3584.
8. Wierzbiicki R, Jonker DJ, Moore MJ, et al. A phase II, multicenter study of cetuximab monotherapy in patients with refractory, metastatic colorectal carcinoma with absent epidermal growth factor receptor immunostaining. *Invest New Drugs*. 2011;29:167–174.
9. Hartmann S, Seher A, Brands RC, et al. Influence of epidermal growth factor receptor expression on the cetuximab and panitumumab response rates of head and neck carcinoma cells. *J Craniomaxillofac Surg*. 2014;42:1322–1328.
10. Zips D, Zophel K, Abolmaali N, et al. Exploratory prospective trial of hypoxia-specific PET imaging during radiochemotherapy in patients with locally advanced head-and-neck cancer. *Radiother Oncol*. 2012;105:21–28.
11. Hoeben BA, Troost EG, Span PN, et al. ^{18}F -FLT PET during radiotherapy or chemoradiotherapy in head and neck squamous cell carcinoma is an early predictor of outcome. *J Nucl Med*. 2013;54:532–540.
12. Paidpally V, Tahari AK, Lam S, et al. Addition of ^{18}F -FDG PET/CT to clinical assessment predicts overall survival in HNSCC: a retrospective analysis with follow-up for 12 years. *J Nucl Med*. 2013;54:2039–2045.
13. van Dijk LK, Hoeben BA, Stegeman H, et al. ^{111}In -cetuximab-F(ab')₂ SPECT imaging for quantification of accessible epidermal growth factor receptors (EGFR) in HNSCC xenografts. *Radiother Oncol*. 2013;108:484–488.
14. van Dijk LK, Hoeben BA, Kaanders JH, Franssen GM, Boerman OC, Bussink J. Imaging of epidermal growth factor receptor expression in head and neck cancer with SPECT/CT and ^{111}In -labeled cetuximab-F(ab')₂. *J Nucl Med*. 2013;54:2118–2124.
15. Hoeben BA, Molkenboer-Kuenen JD, Oyen WJ, et al. Radiolabeled cetuximab: dose optimization for epidermal growth factor receptor imaging in a head-and-neck squamous cell carcinoma model. *Int J Cancer*. 2011;129:870–878.
16. Rademakers SE, Rijken PF, Peeters WJ, et al. Parametric mapping of immunohistochemically stained tissue sections; a method to quantify the colocalization of tumor markers. *Cell Oncol (Dordr)*. 2011;34:119–129.
17. Stegeman H, Span PN, Cockx SC, et al. EGFR-inhibition enhances apoptosis in irradiated human head and neck xenograft tumors independent of effects on DNA repair. *Radiat Res*. 2013;180:414–421.
18. Bussink J, van der Kogel AJ, Kaanders JH. Activation of the PI3-K/AKT pathway and implications for radioresistance mechanisms in head and neck cancer. *Lancet Oncol*. 2008;9:288–296.
19. Kriegs M, Kasten-Pisula U, Rieckmann T, et al. The epidermal growth factor receptor modulates DNA double-strand break repair by regulating non-homologous end-joining. *DNA Repair (Amst)*. 2010;9:889–897.
20. Dittmann K, Mayer C, Fehrenbacher B, et al. Radiation-induced epidermal growth factor receptor nuclear import is linked to activation of DNA-dependent protein kinase. *J Biol Chem*. 2005;280:31182–31189.
21. Stegeman H, Kaanders JH, van der Kogel AJ, et al. Predictive value of hypoxia, proliferation and tyrosine kinase receptors for EGFR-inhibition and radiotherapy

- sensitivity in head and neck cancer models. *Radiother Oncol.* 2013;106:383–389.
22. Weinstein IB, Joe A. Oncogene addiction. *Cancer Res.* 2008;68:3077–3080.
 23. van Dijk LK, Boerman OC, Franssen GM, Lok J, Kaanders JH, Bussink J. Early response monitoring with ¹⁸F-FDG PET and cetuximab-F(ab')₂-SPECT after radiotherapy of human head and neck squamous cell carcinomas in a mouse model. *J Nucl Med.* 2014;55:1665–1670.
 24. Mendelsohn J, Baselga J. Status of epidermal growth factor receptor antagonists in the biology and treatment of cancer. *J Clin Oncol.* 2003;21:2787–2799.
 25. Yoshida T, Okamoto I, Okabe T, et al. Matuzumab and cetuximab activate the epidermal growth factor receptor but fail to trigger downstream signaling by Akt or Erk. *Int J Cancer.* 2008;122:1530–1538.
 26. Cohen EE, Rosen F, Stadler WM, et al. Phase II trial of ZD1839 in recurrent or metastatic squamous cell carcinoma of the head and neck. *J Clin Oncol.* 2003;21:1980–1987.
 27. Chung KY, Shia J, Kemeny NE, et al. Cetuximab shows activity in colorectal cancer patients with tumors that do not express the epidermal growth factor receptor by immunohistochemistry. *J Clin Oncol.* 2005;23:1803–1810.
 28. Wheeler DL, Dunn EF, Harari PM. Understanding resistance to EGFR inhibitors-impact on future treatment strategies. *Nat Rev Clin Oncol.* 2010;7:493–507.
 29. Yamatodani T, Ekblad L, Kjellen E, Johnsson A, Mineta H, Wennerberg J. Epidermal growth factor receptor status and persistent activation of Akt and p44/42 MAPK pathways correlate with the effect of cetuximab in head and neck and colon cancer cell lines. *J Cancer Res Clin Oncol.* 2009;135:395–402.
 30. Janmaat ML, Kruyt FA, Rodriguez JA, Giaccone G. Response to epidermal growth factor receptor inhibitors in non-small cell lung cancer cells: limited antiproliferative effects and absence of apoptosis associated with persistent activity of extracellular signal-regulated kinase or Akt kinase pathways. *Clin Cancer Res.* 2003;9:2316–2326.
 31. Schöder H, Fury M, Lee N, Kraus D. PET monitoring of therapy response in head and neck squamous cell carcinoma. *J Nucl Med.* 2009;50(suppl 1):74S–88S.
 32. Castaldi P, Rufini V, Bussu F, et al. Can “early” and “late” ¹⁸F-FDG PET-CT be used as prognostic factors for the clinical outcome of patients with locally advanced head and neck cancer treated with radio-chemotherapy? *Radiother Oncol.* 2012;103:63–68.
 33. Hentschel M, Appold S, Schreiber A, et al. Early FDG PET at 10 or 20 Gy under chemoradiotherapy is prognostic for locoregional control and overall survival in patients with head and neck cancer. *Eur J Nucl Med Mol Imaging.* 2011;38:1203–1211.